ELSEVIER

Seminars in
NUCLEAR
MEDICINE

Computer-Aided Diagnosis and Artificial Intelligence in Clinical Imaging

Junji Shiraishi, PhD, Qiang Li, PhD, Daniel Appelbaum, MD, and Kunio Doi, PhD

Computer-aided diagnosis (CAD) is rapidly entering the radiology mainstream. It has already become a part of the routine clinical work for the detection of breast cancer with mammograms. The computer output is used as a "second opinion" in assisting radiologists' image interpretations. The computer algorithm generally consists of several steps that may include image processing, image feature analysis, and data classification via the use of tools such as artificial neural networks (ANN). In this article, we will explore these and other current processes that have come to be referred to as "artificial intelligence." One element of CAD, temporal subtraction, has been applied for enhancing interval changes and for suppressing unchanged structures (eg, normal structures) between 2 successive radiologic images. To reduce misregistration artifacts on the temporal subtraction images, a nonlinear image warping technique for matching the previous image to the current one has been developed. Development of the temporal subtraction method originated with chest radiographs, with the method subsequently being applied to chest computed tomography (CT) and nuclear medicine bone scans. The usefulness of the temporal subtraction method for bone scans was demonstrated by an observer study in which reading times and diagnostic accuracy improved significantly. An additional prospective clinical study verified that the temporal subtraction image could be used as a "second opinion" by radiologists with negligible detrimental effects. ANN was first used in 1990 for computerized differential diagnosis of interstitial lung diseases in CAD. Since then, ANN has been widely used in CAD schemes for the detection and diagnosis of various diseases in different imaging modalities, including the differential diagnosis of lung nodules and interstitial lung diseases in chest radiography, CT, and position emission tomography/CT. It is likely that CAD will be integrated into picture archiving and communication systems and will become a standard of care for diagnostic examinations in daily clinical work.
Semin Nucl Med 41:449-462

Computer-aided diagnosis (CAD) has become a part of the routine clinical work for detection of breast cancer on mammograms at many screening sites and hospitals[1-13] in the United States. It is likely that CAD will be applied widely in the detection and differential diagnosis of many different types of abnormalities[14-26] in medical images by use of various imaging modalities, including nuclear medicine. Although early attempts at computerized analysis of medical images[27-33] were made in the 1960s, a serious and large-scale systematic investigation on CAD began in the early 1980s at the Kurt Rossmann Laboratories for Radiologic Image Research in the Department of Radiology at the University of Chicago, with a fundamental change in the concept for the use of the computer output, from automated computer diagnosis to computer-aided diagnosis.[21-26] The computer output for CAD is used as a "second opinion" in assisting radiologists' image interpretations. The computer algorithm generally consists of several steps, which may include image processing, image feature analysis, and data classification by use of tools, such as artificial neural networks (ANN); these may be referred to as artificial intelligence.

Most publications on CAD have been concerned with 3 organs—the chest, breast, and colon—but other organs,

Kurt Rossmann Laboratories for Radiologic Image Research, Department of Radiology, the University of Chicago, Chicago, IL.
Current address for Junji Shiraishi: Faculty of Life Sciences, Kumamoto University, 4-24-1 Kuhonji, Kumamoto, Kumamoto 862-0976 Japan.
Current address for Qiang Li: Carl E. Ravin Advanced Imaging Laboratories, Department of Radiology, Duke University, Erwin Road, Suite 302, Durham, NC 27705.
Current address for Kunio Doi: Gunma Prefectural College of Health Sciences, 323-1 Kamiokimachi, Maebashi, Gunma 371-0052, Japan.
Address reprint requests to Daniel Appelbaum, Kurt Rossmann Laboratories for Radiologic Image Research, Department of Radiology, the University of Chicago, 5841 South Maryland Avenue, Chicago, IL 60637. E-mail: dappelbaum@radiology.bsd.uchicago.edu

0001-2998/11/$-see front matter
doi:10.1053/j.semnuclmed.2011.06.004

such as brain, liver, and skeletal and vascular systems, also have been subjected to CAD research. The detection of cancer in the breast,[1-13] lung,[34-40] and colon[41,42] is commonly achieved through screening examinations.[43] A great fraction of these examinations produce normal results, and the detection of only a small number of suspicious lesions by radiologists is considered both difficult and time-consuming. Therefore, it appears reasonable that the initial phase of practical CAD in clinical situations has begun in these screening examinations, and commercial CAD systems for detection of these cancers are now available for clinical use. However, it is expected that, in the future, many CAD schemes for detection and/or differential diagnosis will be developed for clinical use in various fields. In this article, we present a CAD scheme[44] that was developed initially for the detection of interval changes in successive whole-body bone scans in nuclear medicine and that subsequently has been used as a routine clinical tool based on encouraging results obtained from observer tests[45] and prospective studies.[46] We also present another CAD scheme[47] for the distinction between benign and malignant pulmonary nodules by use of ANN and image information obtained from positron-emission tomography (PET) and computed tomography (CT).

Detection of Interval Changes in Successive Whole-Body Bone Scans

Temporal Subtraction Method

To use CAD systems in practice in clinical situations, the radiologist must trust and feel comfortable with the CAD output. One effective approach to be used in the CAD system for satisfying this requirement is to imitate radiologists' procedures for interpreting medical images. When the patient has a previous image available, radiologist commonly compare the sequence of 2 images for detecting interval changes. In this comparative interpretation, radiologists use the previous image as a mask image to enhance any potential interval changes on the current image. Temporal subtraction has been developed for computerizing the radiologists' masking procedure, resulting in improved decision-making and reduced reading times.

The development of the temporal subtraction method originated with chest radiographs.[48] Note that the clinical utility of the temporal subtraction method is particularly efficient when the same radiological examination is performed frequently for one patient, so that there is a greater likelihood for patients to have more than 2 sequential images for the interpretation. Therefore, the chest radiograph was very appropriate for introducing the temporal subtraction method. However, because precise patient positioning for each chest radiograph is somewhat variable, a simple subtraction technique could not be used for temporal subtraction. Therefore, a nonrigid image-matching technique for 2 sequential images was developed. Figure 1 illustrates a nonrigid image-matching technique called nonlinear image warping. In this technique, a 2-dimensional polynomial warping surface was obtained with shift values of the x, y coordinates based on a cross-correlation value for each pair of corresponding small regions of interest (ROIs).[48]

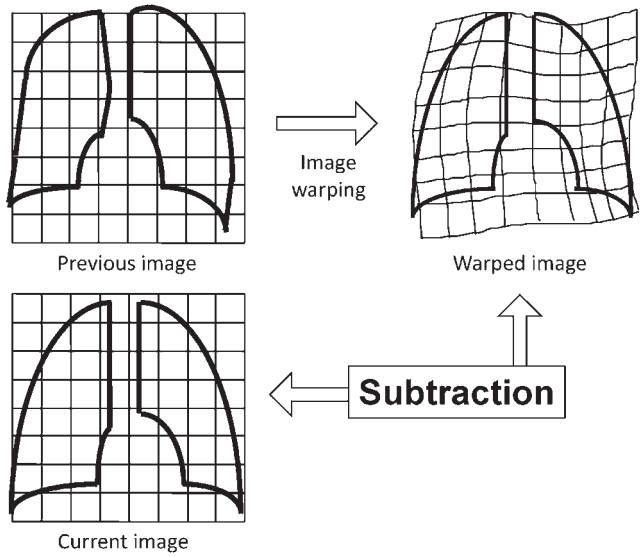

Figure 1 Concept of nonrigid image warping technique for temporal subtraction method in successive chest radiography.

After the first attempt at temporal subtraction with chest radiography was successfully completed and the usefulness of this method was demonstrated by observer study,[49-51] several improvements in the reduction of misregistration artifacts were developed.[52,53] Figure 2 shows one clinical case of a pair of chest radiographs in which the temporal subtraction method worked efficiently for identifying a new interval change. Recently, temporal subtraction methods were introduced into successive chest CT scans.[54,55] In the newest temporal subtraction method,[55] volume CT data were nonlinearly warped and matched by use of a voxel-matching technique (Fig. 3). Because the clinical utility of chest CT screening for lung cancer has been demonstrated,[56] such temporal subtraction methods for chest CT will likely be in demand soon.

Development of Temporal Subtraction Method for Whole-Body Bone Scans

Bone scintigraphy is one of the most frequent examinations among various diagnostic nuclear medicine procedures and is often repeated regularly on the same patient who requires periodic monitoring to identify disorders, such as skeletal metastases, primary bone tumors, and osteomyelitis. In general, bone scans are used for imaging of new bone formation that may occur because of the presence of almost any skeletal pathology and for demonstrating increased and/or decreased gamma ray emissions localized to the site of bone abnormalities by use of the radiopharmaceutical technetium-99m methylene diphosphonate or hydroxymethane diphosphonate. The sensitivity of bone scan examinations for detection of bone abnormalities has been considered very high; however, it is time-consuming to identify multiple lesions, such as bone metastases of prostate and breast cancers. In addi-

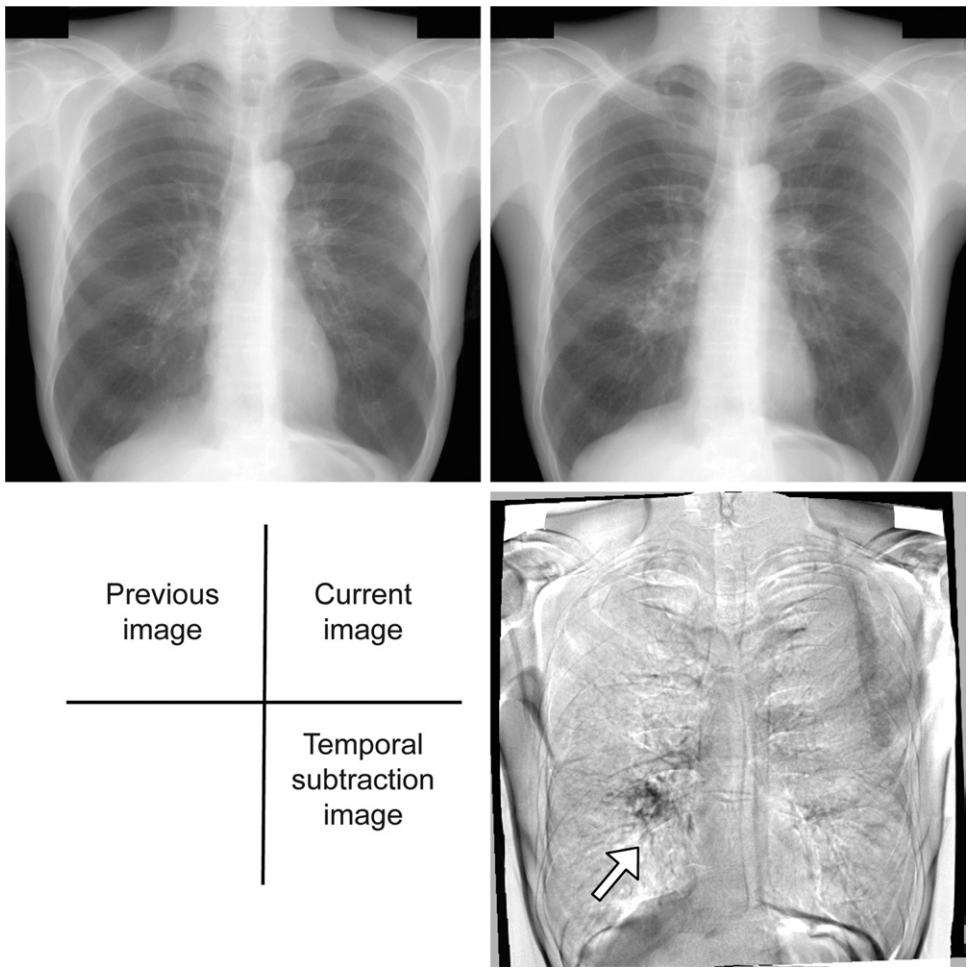

Figure 2 Example of temporal subtraction image in 2 sequential chest radiographs. Progression of a lung mass in right lower lung was clearly identified in the temporal subtraction image.

tion, because of variations in patient positioning, the distribution of the radioisotope during each examination and the fluctuating image quality of gamma cameras, it is difficult to detect subtle changes between 2 successive abnormal bone scans, particularly in patients who have many lesions. Therefore, a temporal subtraction method that can assist radiologists in the detection and/or quantification of interval changes in successive bone scans would be useful by reducing the interpretation time and by quantifying the extent of an increase and/or a decrease in the radioisotope uptake on serial bone scans.[44]

Image Database and Computerized Method[44]

For developing a computerized scheme of applying temporal subtraction to successive bone scans, we used 58 pairs of successive bone scans, each of which included both posterior and anterior views obtained simultaneously by use of a set of 2 gamma cameras placed face-to-face. The 58 cases were carefully selected with several inclusion criteria determined by 2 radiologists, as follows: (1) at least one abnormal finding in either view, (2) a maximum number of 20 interval changes, and (3) one image pair per patient. To determine a "reference standard" for interval changes for all cases, we performed an observer study in which we identified interval changes in either a hot lesion (uptake was increased compared with the previous scan or there was new uptake in the current scan) or a cold lesion (uptake was decreased or disappeared). On the basis of agreement of the 3 radiologists who participated in the observer study, we determined 107 "reference standard" interval changes, which included 71 hot lesions and 36 cold lesions for anterior and posterior views. The average number of interval changes was 1.85 (range, 0-11), and 17 of the 58 pairs had no interval change, whereas all cases included one or more abnormalities in at least one view.

Figure 4 illustrates an overall computerized scheme of a temporal subtraction method for the detection of interval changes on successive whole-body bone scan pairs. For application of a nonlinear image-warping technique[53] to the temporal subtraction method, the grayscale of each image was normalized first, and then the size, orientation, and grayscale of a previous image were adjusted to match those of a current image.

Because of residual radioactive urine in the bladder and/or leakage at the injection site, bone-scan images frequently had extremely high intensities in their raw image data. Therefore, all input images for the computerized scheme were converted

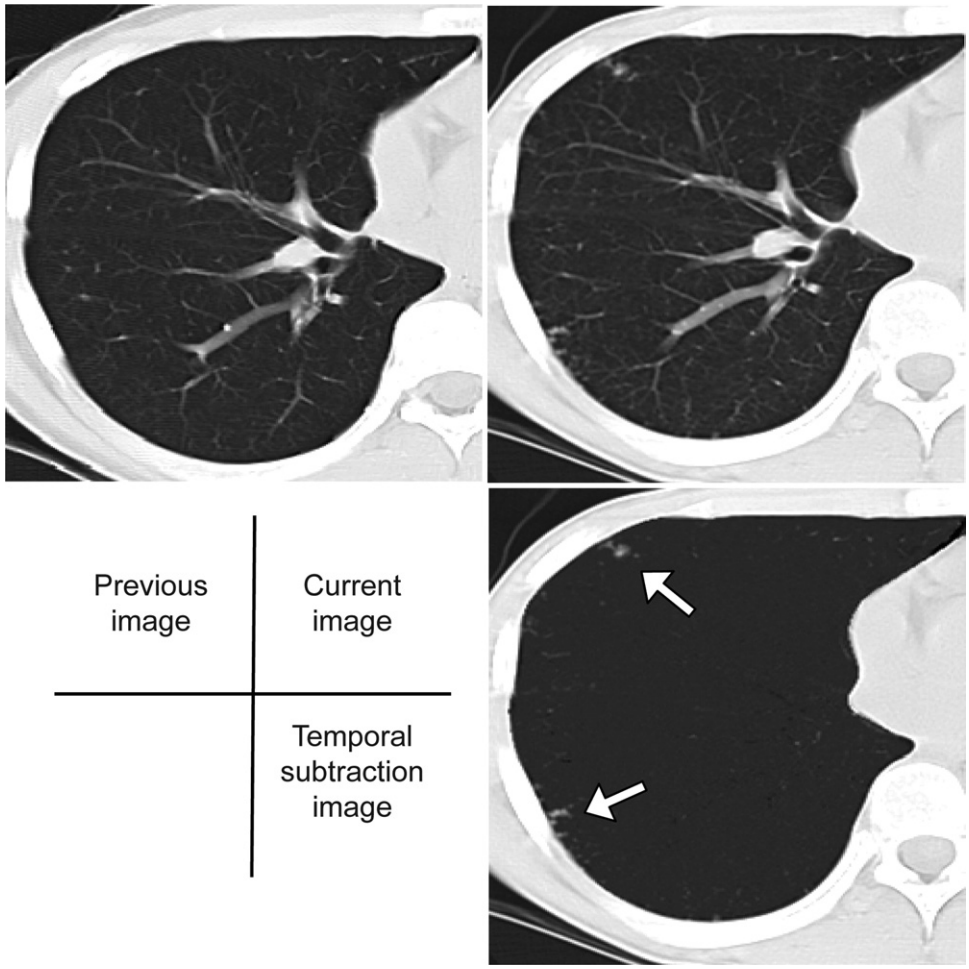

Figure 3 Example of temporal subtraction image in 2 sequential CTs with 2 small lung nodules (arrow). Because a voxel-matching technique searched matched pixels on neighbors in detail, normal lung structures, such as pulmonary vessels and bronchi, were removed clearly in the temporal subtraction image.

in advance from the original grayscale (16-bit) of each of the raw image data by use of a histogram analysis for removal of areas with extremely high intensities. In the next step, the previous image was matched to the current image in the image size, orientation, and grayscale so that we could minimize the difference between the 2 images for visual comparison and so that we could apply a nonlinear image-warping technique for obtaining the temporal subtraction image. The grayscale of the previous image was matched to that of the current image by analysis of the correlation between the average pixel values of the corresponding small ROIs in the 2 images. The slope and the intersection of a regression line for the relationship between the average pixel values in the previous and the current images were used for linearly converting the pixel values of the previous image. Then, we used a nonlinear image-warping technique that was developed for the contralateral subtraction technique in chest radiographs[53] for further matching of the 2 images.

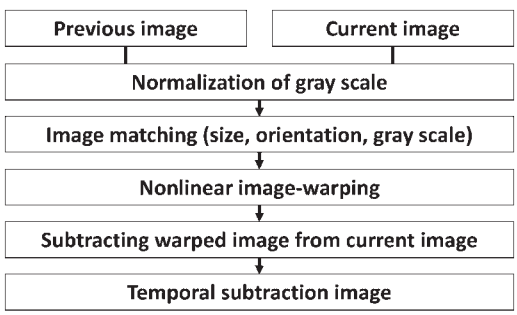

Figure 4 Overall computerized schemes for the temporal subtraction method in successive whole-body bone scans.

A modified nonlinear image-matching technique for whole-body bone scans consisted of 3 steps: (1) global matching between the 2 images, (2) leg matching between the 2 images, and (3) local image matching and warping by use of an elastic matching technique. The purpose of global matching is to register the previous and current images approximately so the subsequent local matching and image-warping technique can provide improved subtraction images and can also be more efficient. After the global matching, the 2 images are registered approximately. However, the corresponding legs in the 2 images are often still far from each other in the horizontal direction, which makes the matching of the legs in the 2 images very difficult and makes the legs the

main source of misregistration artifacts. To address this problem, we attempted to match the legs approximately in the 2 images with a simple technique which shifted each line of each leg horizontally, one leg at a time.

Finally, the local image-matching and -warping technique tries to register accurately the 2 images that are roughly matched by use of global matching and leg matching. In this technique, an elastic matching technique[53] was applied for the final determination of shift vectors which were initially calculated on the basis of cross-correlation values between template ROIs and the corresponding search area ROIs located on the previous and the current image, respectively. A shift vector indicates a shift in the location of a template ROI (12 × 12 pixels) to be matched with a corresponding local region (12 × 12 pixels) included in the search area ROI (24 × 24 pixels), and a correlation value indicates the extent of the similarity between the shifted template and the corresponding region of the search area. Once the final shift vectors for all ROIs had been obtained, a bilinear interpolation technique was used to determine the shift vectors for all pixels over the entire previous image. The interpolated shift vectors were then used for warping of the previous image.

The warped previous image was then subtracted pixel-by-pixel from the original image to provide the temporal subtraction image. To indicate both hot and cold regions in the temporal subtraction image, we added the base pixel value of 256 (25% of the maximum gray scale) to the subtraction image. Figure 5 shows posterior views of the original (Fig. 5A), the matched (Fig. 5B), and the warped image of the previous scan (Fig. 5C), which was subtracted from the current scan (Fig. 5D) to provide the temporal subtraction image (Fig. 5E).

Observer Study for the Detection of Interval Changes in Successive Whole-Body Bone Scans Without and with Temporal Subtraction Images

To evaluate the usefulness of the temporal subtraction method in an improvement in radiologists' diagnostic accuracy in detecting interval changes and a reduction in reading time, an observer performance study with a jackknife free-response receiver operating characteristic (ie, JAFROC) analysis method[57-59] was conducted.[45] Twenty pairs of successive whole-body bone scans were randomly selected from 58 bone scintigrams. On the basis of the 2 radiologists' agreement on both the location and the type of each lesion, we determined 72 "reference standard" interval changes, which included 64 lesions of increased intensity and 8 lesions of decreased intensity on anterior and/or posterior views. The average number of interval changes was 3.6 (range, 0-11); 3 of the 20 pairs had no interval change even if all cases included one or more abnormalities in at least one view. In addition, we selected another 5 cases from the original 58 to be used as a training set for the observer performance study. These 5 training cases included 19 interval changes (average, 3.6; range, 0-7).

Five radiologists, including 3 attendings and 2 residents, participated in the observer study. All the radiologists were trained to interpret bone scans and/or had clinical experience in nuclear medicine. The observer study was organized into 2 reading sessions separated by an interval of at least two weeks. In the first session, without temporal subtraction images, the previous and current images were shown to the radiologist, and then he or she marked the lesion locations on the current images and provided confidence ratings on potential interval changes by observing the previous images. In

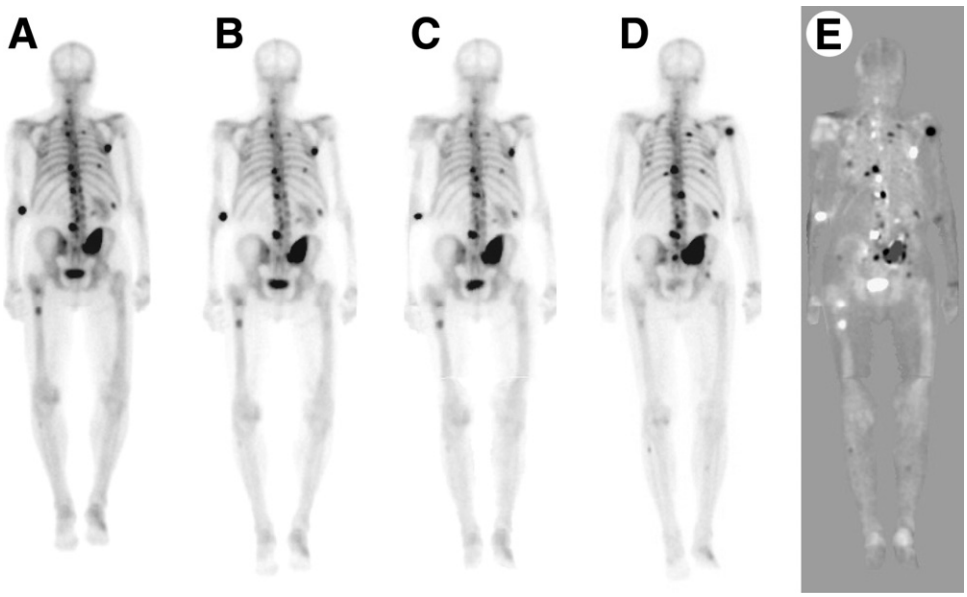

Figure 5 Example of posterior views of (B) matched and (C) nonlinearly warped images of (A) previous image, which was subtracted from (D) current image to provide (E) temporal subtraction image.

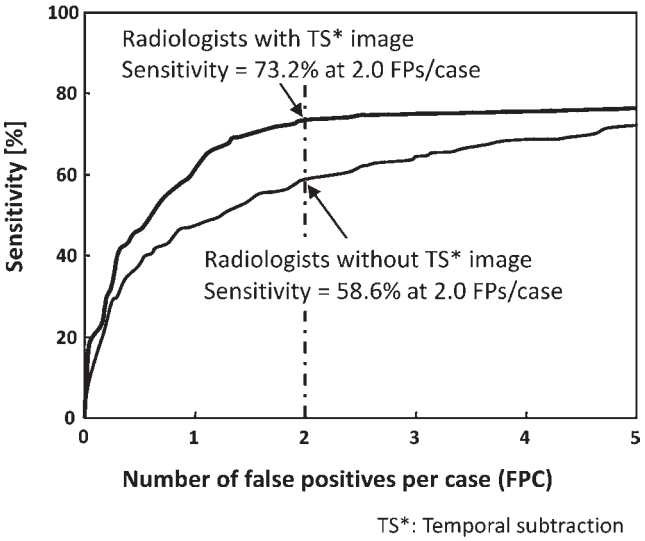

Figure 6 Average FROC curves for the 5 radiologists' performance in the detection of interval changes in 20 successive whole-body bone scans without and with TS images.

the second session, temporal subtraction images were shown together with the modified previous and current images, and the radiologist was asked again to mark lesion locations and give their ratings.

The average free-responce receiver operating characteristic (FROC) curves for all radiologists were used for comparison of the radiologists' performance with regard to the sensitivity for the detection of interval changes at a specific false-positive level (eg, 2.0 false-positive results per case) without and with temporal subtraction images. A pseudovalue matrix with a sequence of figure-of-merit values (the analog of the area under the ROC curves) for JAFROC analysis (method 1) was analyzed by the use of an analysis of variance techniques[60] for estimating statistically significant differences between the 2 FROC data sets obtained without and with the temporal subtraction image. The average sensitivity for detecting interval changes was improved significantly by use of temporal subtraction images from 58.6% to 73.2% at a false-positive rate of 2.0 per case on the average FROC curves, as shown in Fig. 6. For these FROC data, the average figure-of-merit values for all radiologists increased to a statistically significant degree, from 0.508 without the temporal subtraction images to 0.613 with the images ($P = 0.035$). Moreover, the performance of every radiologist was improved when the temporal subtraction image was used. The mean reading time per case was reduced significantly from 134 seconds to 91 seconds ($P = 0.004$). In addition, the reading time was reduced significantly for 4 of the 5 radiologists, with more than a 20% reduction in reading times.

Prospective Clinical Study for Evaluating the Clinical Utility of Temporal Subtraction Images

After the demonstration of usefulness of the temporal subtraction method in the aforementioned observer study, a prospective clinical study for evaluating the clinical utility of the temporal subtraction method was performed.[46] For the prospective clinical study, we developed a temporal subtraction image server that included 5 functions: (1) an automated image-retrieval system for searching the most recent whole-body bone scan images in picture archiving and communication systems (PACS); (2) an automated image-conversion system for converting several types of image formats into raw image data with a 256 × 1024 matrix size; (3) an automated temporal subtraction image-production system; (4) a computer interface for displaying and evaluating temporal subtraction images together with the routine diagnosis by use of PACS; and (5) an automated data-archiving system by securing patient identification.

This clinical study was approved by the institutional review board of the University of Chicago. With this approval, the temporal subtraction images of a patient were used only when his/her consent was obtained. The radiologist could revise his/her report after reviewing the temporal subtraction images if the findings on the temporal subtraction images were confirmed retrospectively on our clinical PACS. In the standard reading without temporal subtraction images, the radiologist made his/her initial decision regarding bone-scan scintigrams by using a standard PACS viewer as usual, and he/she dictated the findings (or reviewed them with a resident to dictate). After the standard reading, the radiologist was required to read the case again along with the temporal subtraction images immediately after the completion of the initial reading. During the second reading with the temporal subtraction images, the radiologist referred to his/her original assessments to confirm his/her impression from the temporal subtraction images.

Immediately after the second reading, to evaluate the clinical utility of temporal subtraction images, the radiologist ranked the overall utility of temporal subtraction images on a discrete 5-point scale (ie, extremely beneficial, somewhat beneficial, no utility, somewhat detrimental, and extremely detrimental). In addition, the overall utility was evaluated and graded with several reasons, such as "change in impression," "increase/decrease in confidence," "change in findings," or "the potential to increase/reduce the reading time." Finally, to estimate the utility of temporal subtraction images in actual clinical actions, we also asked the radiologist whether the use of temporal subtraction images changed his/her original impression in the report (eg, stable osseous metastases, progression of osseous metastases). However, for the radiologist to change the original report after a review of the temporal subtraction images, we asked him/her to confirm his/her judgment by using the clinical PACS for viewing the original bone scans as well as static images of lesions of interest. In addition, a consensus for all cases with a changed impression was made retrospectively by a panel of 2 radiologists who specialized in nuclear medicine, to confirm that the newly observed findings were real, and that they were not unduly biased by use of temporal subtraction images.

The prospective study was performed between November 22, 2006, and November 30, 2008, at the University of Chicago Hospital. We had 256 consenting patients, of whom 143 had one or more pairs of whole-body bone scans avail-

able for temporal subtraction images. For the 143 patients who had given consent, there were 304 pairs of bone scans. We obtained temporal subtraction images successfully in 292 (96.1%) pairs and failed to produce temporal subtraction images in 12 pairs. There was one pair of whole-body bone scans available for temporal subtraction images in 69 patients, and there were 2 pairs for 28, 3 for 26, 4 for 9, and 5 or more for 11 (n = 304). The average number of pairs available for temporal subtraction images per patient was 2.1, and the maximum number of pairs was 8 during the period of our prospective study.

Radiologists' subjective ratings for the clinical utility of temporal subtraction images applied to the 292 pairs of successive bone scans indicated that temporal subtraction images were considered as "extremely beneficial (n = 24)" or "somewhat beneficial (n = 223)" in 247 (84.6%) pairs of these bone scans, whereas they were considered as having "no utility" in 44 pairs, and as "somewhat detrimental" in only one pair. No case was considered "extremely detrimental." The radiologists changed the final impression of their initial report in 18 pairs of successive bone scans (6.2%) among the 292 pairs. All changes made by use of temporal subtraction images were retrospectively confirmed as "correct responses" by the consensus of 2 expert radiologists. Figure 7A-B shows examples of clinical cases that demonstrated the clinical utility of the temporal subtraction method.

In conclusion, the usefulness of temporal subtraction images in successive whole-body bone scans was demonstrated in its clinical utility in the prospective clinical study. With further refinement and validation, the temporal subtraction image could, with negligible detrimental effects, likely be used as an inexpensive "second opinion" by radiologists, increasing their accuracy, speed, and confidence in the interpretation of whole-body bone scans.

CAD for the Detection of Interval Changes with Temporal Subtraction Images Between Successive Whole-Body Bone Scans

Although a temporal subtraction image alone could be effective for aiding radiologists in interpretation of interval changes in successive whole-body bone scans, a computerized scheme to highlight interval changes on temporal subtraction images could be of additional value to radiologists, particularly those not experienced in the use of temporal subtraction. Therefore, a computerized scheme for the detection of interval changes was developed simultaneously with the development of the temporal subtraction method.[44] Figure 8 shows an overall scheme of the computerized scheme that consists of 4 steps: (1) initial identification of candidates for interval changes, (2) image feature extraction of candidates for interval changes, (3) removal of some false positives by use of a rule-based test, and (4) display of the computer output for identified interval changes. In this computerized scheme, 2 types of interval changes, for hot and cold lesions, were identified separately by use of the same techniques, but with different parameters. In addition, all the procedures in the computerized scheme were performed separately for each view, and the overall performance for the detection of interval changes was evaluated on the basis of the number of "reference standard" interval changes included in each case. Note that, in the temporal subtraction images, hot lesions appear as dark areas, whereas cold lesions appear as light areas. Therefore, hot-lesion images were created by elimination of cold lesions, ie, by changing the pixel values in cold lesions to the base pixel value of 256. By contrast, cold-lesion images were created by reversing of the pixel values in the temporal subtraction image such that cold legions appeared as dark areas and hot lesions as light areas. Then, cold-lesion images were obtained by elimination of light areas in the same way as that used for hot-lesion images.

Candidates for interval changes in each view were identified initially by use of a multiple thresholding technique[61] for hot-lesion−enhanced and cold-lesion−enhanced images, which were obtained from the hot-lesion and cold-lesion images, respectively. The grayscales of the hot-lesion−enhanced and the cold-lesion−enhanced images were normalized linearly by use of the upper 5% and 85% of the area under the histogram of pixel values included in the image. In addition, we applied a Gaussian filter to the images to reduce some of the remaining noise. Initial candidates of interval changes were identified if (1) the centroid of the candidate, which is called an island here and is derived by multiple-gray-level thresholding, was not overlapped with the candidates identified in the previous threshold levels; and (2) if the effective diameter of the island was between 3.0 and 200.0 mm.

In the process of initial identification, we obtained 10 image features on the basis of the contour of an island in the hot-lesion/cold-lesion enhanced image, including: (1) threshold value [%] at the initial identification level, (2) sequential order of the candidate among all the candidates detected initially, (3) effective diameter,[61] (4) circularity,[61] (5) irregularity,[61] (6) normalized vertical location, (7) contrast value obtained by the difference between the maximum and the minimum pixel values within the island, (8) average pixel value within the island, (9) standard deviation of pixel values within the island, and (10) difference in the pixel value between the inside and outside regions of the island. In addition to the 10 initial image features obtained from the temporal subtraction images, we obtained 4 image features (the contrast, average pixel value, standard deviation of the pixel value, and the difference between the inside and outside regions) from the warped previous image and also from the current image at the locations of identified candidates to examine the pixel values and image features in the original images.

We applied a rule-based scheme[62] for removal of several false-positive results in each view. A number of image feature pairs were determined for both hot and cold lesions by use of a 2-dimensional linear discriminant analysis method. The 2-dimensional linear discriminant analysis method was first trained by use of all the 58 case pairs and then was tested by use of the same case pairs. When all candidates, which were

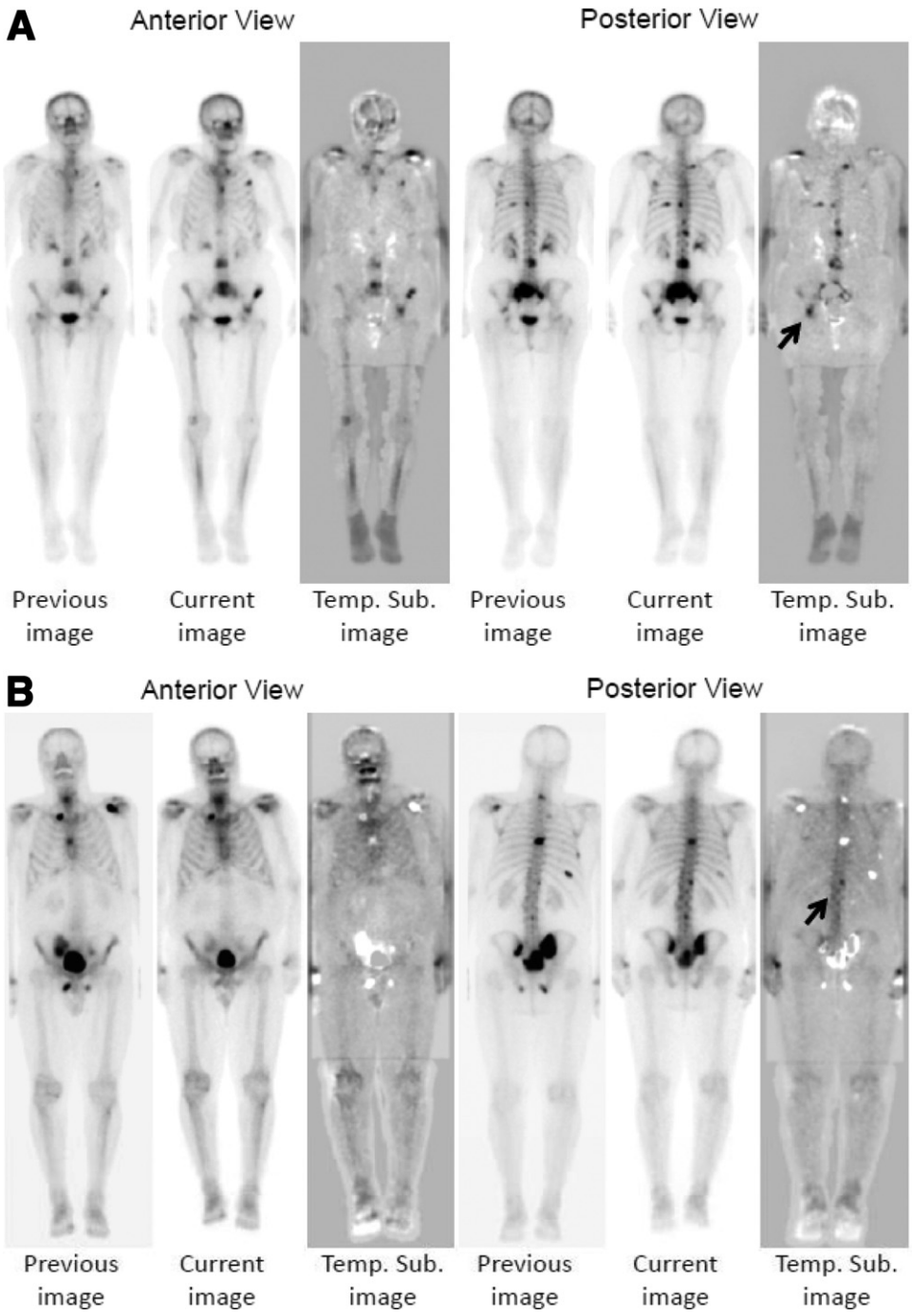

Figure 7 Examples of clinical cases obtained in the prospective clinical study. (A) These bone scans were performed for metastatic evaluation in a 72-year-old woman with breast cancer. Although the follow-up scan was initially interpreted as stable disease, there had actually been slight progression (arrow) to several the lesions. These changes became obvious on the temporal subtraction images. (B) These bone scans were also performed for metastatic evaluation in a 73-year-old man with prostate carcinoma. Since the follow-up scan was initially interpreted as improvement of all lesions, the temporal subtraction images revealed a subtle increasing focus at T12 (arrow) suspicious for progression of disease at this site.

identified in each view, were combined, some lesions were identified in both views because of their high intensities for both anterior and posterior views. In this study, an interval change was considered a true positive when the lesion was identified in either view, even if the reference standard was marked in both views by the radiologists. The overall sensitivity in the detection of interval changes, including both hot and cold lesions, in 58 successive bone scan pairs, was 95.3% with 5.78 false positives per view.[44] Figure 9 shows an example of previous and current bone scans and their temporal subtraction image with and without the computer marks obtained by this computerized scheme. Note that red and blue

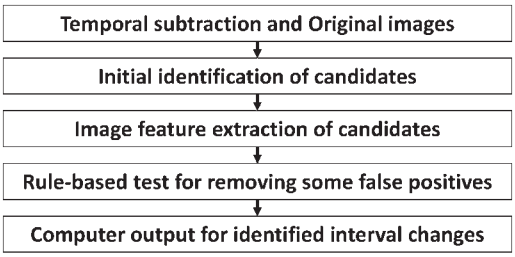

Figure 8 Overall computerized scheme for the detection of interval changes on temporal subtraction image between 2 successive whole-body bone scans.

marks indicate candidates for hot lesion and cold lesion, respectively. Although it was difficult to distinguish 5 metastases on the right ribs as progression or as stable, the temporal subtraction image and its computer marks clearly indicated one metastasis with progression and 4 metastases with regression.

ANN in Computer-Aided Diagnosis

An ANN is a nonlinear computational model that emulates a biological neural network for processing of information. It is one of the most useful and successful computational models in artificial intelligence. When used appropriately, an ANN can solve very complex problems and produce excellent results that conventional approaches cannot. Therefore, ANNs have been used frequently in various applications, including medical imaging. For example, researchers have used ANNs to detect and diagnose interstitial lung diseases,[62-67] lung cancer,[68-71] breast cancer,[72-76] prostate cancer,[77] and pulmonary embolism.[78,79] Excellent review papers for general ANNs can be found in.[80-83]

An ANN typically consists of a large number of highly interconnected artificial neurons (processing elements) working in parallel to solve specific problems. In most ANN applications, neurons are connected in a feed-forward way and are implemented by software algorithms instead of electronic devices. Figure 10 is a schematic illustration of a feed-forward artificial neural network with 3 layers. The first layer is called the input layer, the second the hidden layer, and the third the output layer. The feed-forward ANNs allow signals to travel only in one way, ie, from the input to the output layer. Feed-forward ANNs can learn very complex relationships between the input neurons and output neurons.

Most ANNs used in artificial intelligence and pattern recognition have architectures similar to that shown in Fig. 10; the major difference is the number of neurons in each layer. For instance, if one plans to use 3 features (diameter, contrast, and degree of circularity) to classify lung nodules into 2 categories (malignant and benign), what he/she needs to do first is to construct an ANN with 3 input neurons to indicate the 3 feature values and one output neuron to indicate the likelihood of being malignant. He/she then needs to train the constructed ANN by using many lung nodules with known features for the input neurons and nodule categories for the output neurons. After appropriate training, the ANN should be able to learn the complex relationship between the fea-

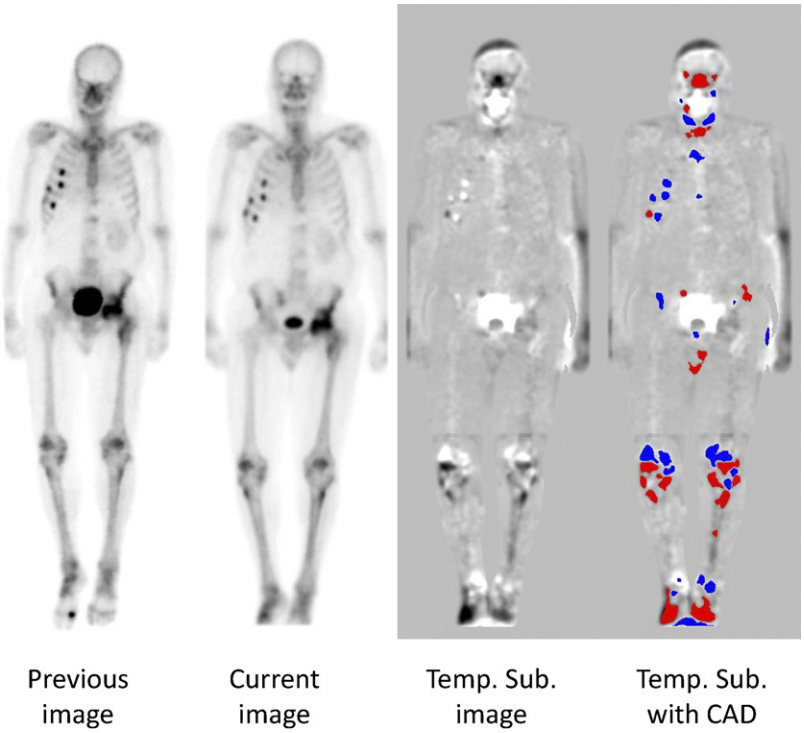

Figure 9 Example of anterior views of previous, current, and temporal subtraction images with and without computer marks of a whole-body bone scan.

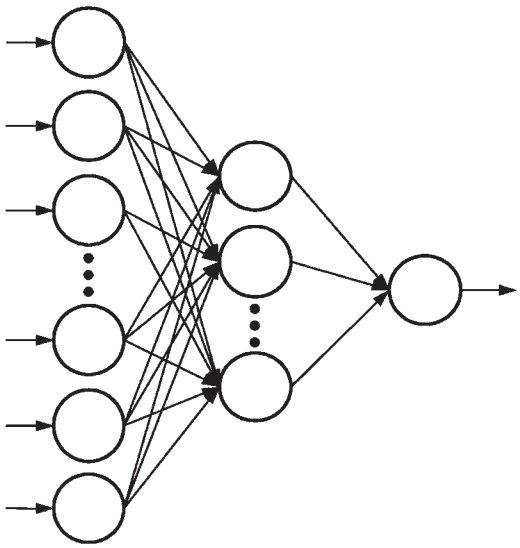

Figure 10 Schematic illustration of a feed-forward artificial neural network with 3 layers. The first layer is called the input layer, the second the hidden layer, and the third the output layer.

tures and the categories and predict the category of a new nodule by using its features.

To our knowledge, an ANN was first used in computer-aided diagnosis for differential diagnosis of interstitial lung diseases in 1990.[62] Since then, ANN has been widely used in CAD schemes for detection and diagnosis of various diseases in different imaging modalities. In this section, we focus on a typical application of ANN in CAD schemes, ie, the differential diagnosis of lung nodules and interstitial lung diseases in chest radiography and computed tomography. We review only ANN-based CAD schemes that used features as the input units of ANNs; ANNs with pixel values as input units are not included in this article.

ANN for Differential Diagnosis of Interstitial Lung Diseases

It is difficult to distinguish accurately between many interstitial lung diseases because they can produce similar or even identical radiographic patterns. Radiologists make a diagnosis by taking into account multiple clinical parameters together with details of the radiographic features. An ANN is an ideal model for integration of many clinical parameters and complex radiographic features. Asada et al[63] first generated 10 hypothetical examples (cases) for each of 9 types of interstitial lung diseases. The 9 types of diseases included sarcoidosis, miliary tuberculosis, lymphangitic metastatic tumor, interstitial pulmonary edema, silicosis, scleroderma, pneumocystis pneumonia, eosinophilic granuloma, and usual interstitial pneumonitis. For each example, they hypothetically created values for 20 features, including 6 clinical parameters and 14 radiographic descriptors. The 6 clinical parameters were the patient's age, sex, duration of symptoms, severity of symptoms, temperature, and immune status. The 14 radiographic descriptors included 6 items regarding the distribution of infiltrates in 6 divisions (upper, middle, and lower zones of the right and left lungs), 5 items relating to details of the infiltrate (homogeneity, fineness or coarseness, nodularity, septal lines, and honeycombing), and 3 additional radiographic variables (lymphadenopathy, pleural effusions, and heart size). Their ANN integrated information on the 20 features to predict the possibilities for each of the 9 types of interstitial lung diseases. Thus, the ANN had 20 input units (features) and 9 output units (diseases). The performance of the ANN in distinguishing between the 9 disease types was evaluated with the area under the receiver operating characteristics curve (AUC). The AUC value of the ANN was 0.967, which was comparable with that of chest radiologists (AUC = 0.967) and superior to that of senior radiology residents (AUC = 0.905). The preliminary results strongly suggest that the ANN has potential utility in the computer-aided differential diagnosis of interstitial lung diseases.

Ashizawa et al[64] extended Asada's work[63] by, including more disease types (from 9 to 11) and more input features (from 20 to 26) for their ANN. Therefore, their ANN had 26 input units (features) and 11 output units (diseases). More importantly, they employed not only 110 hypothetical cases, but also 110 cases from previously published studies and 150 actual clinical cases. The hypothetical cases and published cases were used only for training, whereas the actual clinical cases were used for both training and testing of the ANNs. The ANN validated with actual clinical cases achieved a high performance (AUC = 0.947) for differential diagnosis of 11 interstitial lung diseases.

Ashizawa et al[65] further conducted an observer performance study to evaluate the effect of the ANN output on radiologists' diagnostic accuracy. Thirty-three actual clinical cases (3 cases per disease) were selected for the observer test, and 8 radiologists (4 attending physicians and 4 residents) participated in the study. Each radiologist made a diagnosis first without, and then with, ANN output, which indicated the likelihood of each of the 11 possible diagnoses in each case. By use of the ANN output, the radiologists significantly improved their diagnostic accuracy for interstitial lung diseases from an average AUC of 0.826-0.911 ($P < 0.0001$). This study indicated that the ANN can assist radiologists in the differential diagnosis of interstitial lung disease in chest radiographs.

Abe et al[66] conducted another, similar observer performance study for evaluating the usefulness of the ANN in assisting radiologists diagnose interstitial lung disease in chest radiography. They used 30 difficult cases and asked 5 radiologists to make a differential diagnosis for each case without and with ANN output. The AUC values for the ANN alone, radiologists without ANN output, and radiologists with ANN output were 0.85, 0.81, and 0.87, respectively. By use of the ANN output, radiologists improved their performance compared with ANN alone and radiologists without ANN output.

Fukushima et al[67] further extended Ashizawa's work[64] to high-resolution computed tomography (HRCT). The ANN was designed with 130 cases to differentiate among 11 diffuse interstitial lung diseases by the use of 10 clinical parameters and 23 HRCT features. The ANN thus consisted of 33 input

units and 11 output units, and it achieved an AUC of 0.956. In an observer test, a subset of 45 HRCT cases was selected from the 130 cases, and each HRCT image was viewed by 8 radiologists first without and then with ANN output. The diagnostic performance of 4 chest radiologists and 4 general radiologists was increased by use of the ANN output from 0.986 to 0.992 ($P = 0.071$) and from 0.958 to 0.971 ($P < 0.001$), respectively.

ANN for Differential Diagnosis of Lung Nodules

The ANN was also used for distinguishing between benign and malignant lung nodules. Nakamura et al[68] developed an ANN-based CAD scheme to determine the likelihood of malignancy for lung nodules. The ANN was trained and tested with 56 chest radiographs, which included 34 malignant nodules and 22 benign nodules. Eight subjective image features were evaluated and recorded by 7 radiologists for each nodule, including nodule size, nodule shape, marginal irregularity, spiculation, border definition, lobulation, nodule density, and homogeneity. In addition to the subjective features, 12 objective features were extracted by a computerized method from the nodule outline, which was delineated by radiologists in chest radiography. The 12 objective features included the effective diameter, degree of circularity, degree of ellipticity, the root-mean square variation and the first moment of the power spectrum, degree of irregularity, mean gradient, radial gradient index, tangential gradient index, line enhancement index, and the mean and standard deviation of the pixel value. The authors used 2 clinical parameters (patient's sex and age) together with selected subjective features extracted by radiologists or selected objective features extracted by computer as the input units of the ANN. The sole output unit of the ANN indicated the likelihood of malignancy for a lung nodule. The study indicated that the ANN with clinical parameters and objective features achieved a considerably higher performance (AUC = 0.854) than did the ANN with clinical parameters and subjective features (AUC = 0.761) or radiologists without ANN (AUC = 0.752).

Matsuki et al[69] developed an ANN to differentiate benign from malignant lung nodules on HRCT and evaluated in an observer study the effect of the ANN output on the performance of radiologists. They trained an ANN to distinguish between benign and malignant nodules on 155 lung nodules (99 malignant and 56 benign nodules). They used 7 clinical parameters and 16 subjective radiologic findings extracted by attending radiologists as the input units of the ANN. The ANN achieved a high performance in differentiating benign from malignant lung nodules (AUC = 0.951). In an observer test, the average AUC value for 12 radiologists increased significantly from 0.831 to 0.959 by use of the ANN output.

Whereas the aforementioned ANN schemes were not automated because they used radiologists' subjective ratings as features of lung nodules, Aoyama et al[70] developed an automated ANN scheme to distinguish between benign and malignant lung nodules on chest images. Their database consisted of 55 lung nodules (33 cancers and 22 benign nodules). Each nodule was segmented automatically by analysis of contour lines of the gray-level distribution based on the polar coordinate representation. Seventy-five image features were automatically determined from the nodule outline, the chest image, and histogram analysis of the segmented nodule. Two clinical parameters (age and sex) and 7 image features selected from 75 features were used as the input units for the ANN. The automated ANN showed an improved performance (AUC = 0.872) over that (AUC = 0.854) obtained previously by Nakamura et al[68] with a manual method.

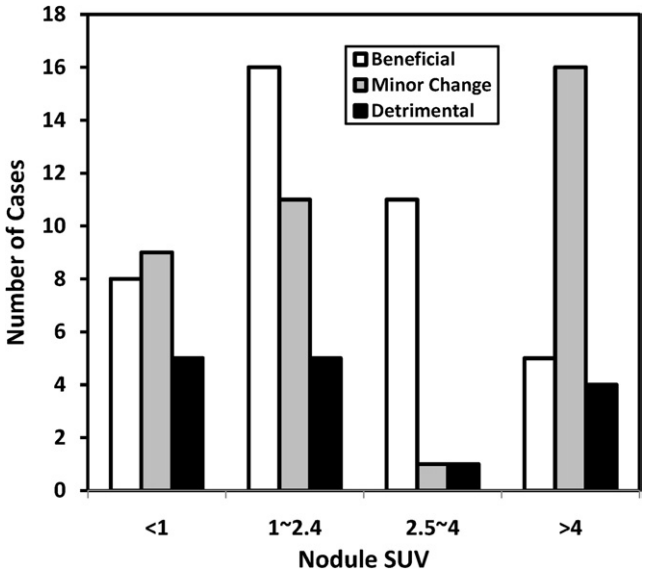

Figure 11 Number of cases with potentially beneficial and detrimental changes (ie, absolute value of change >0.1) and with minor changes (ie, absolute value of change <0.1) in the computer output resulting from use of FDG-PET and additional CT features for nodules in 4 groups of SUV values. The number of cases with beneficial effects resulting from use of additional CT features was greater than that with detrimental effects, especially when the nodule SUV was between 1 and 4.

Artificial Neural Network for Integration of Information from PET and CT

One of the advantages of ANNs is easy integration of information obtained from multiple imaging modalities. Nie et al[47] demonstrated this advantage of ANNs by using ANNs to integrate 18F-fluorodeoxyglucose (FDG) PET and CT information for distinguishing between benign and malignant lung nodules. They retrospectively collected 92 consecutive cases of lung nodules (42 malignant and 50 benign) in patients who underwent both thoracic CT and whole-body 18F-FDG PET/CT. For each patient, they determined 4 clinical parameters (patient's age, sex, smoking status, and history of previous malignancy), 16 subjective CT features on the basis of the size, shape, margin, and internal structure of nodules, and 4 subjective PET features (standard uptake

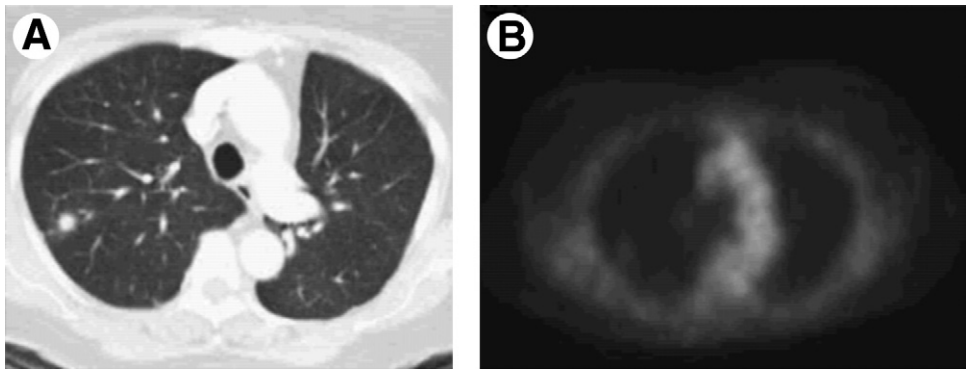

Figure 12 (A) CT and (B) FDG-PET scan of a 69-year-old woman with lung cancer. By use of CT features, the computed likelihood of malignancy was improved (increased) from 0.27 (an indication of a benign nodule, PET alone) to 0.84 (an indication of a malignant nodule, PET + CT).

value, pleural effusion, lymphadenopathy, and extrathoracic malignancy). They then developed and evaluated 3 ANN-based CAD schemes for distinguishing between benign and malignant lung nodules by use of clinical parameters together with CT features, PET features, and both CT and PET features. The ANN with both CT and PET features achieved a significantly higher performance (AUC = 0.95) than that with CT features (AUC = 0.83, $P = 0.015$) or PET features (AUC = 0.91, $P = 0.037$) alone. Therefore, the CAD scheme based on both PET and CT was better able to differentiate benign from malignant lung nodules than were the CAD schemes based on single modalities alone.

To better understand the effect of PET and CT information on nodule characterization, they compared the performance of the CAD scheme by using PET/CT and then using FDG-PET alone for nodules in 4 groups classified according to their standard uptake values (SUVs) of FDG (SUV of <1, 1.1-2.4, 2.5-4, or >4). As shown in Figure 11, of the 47 pulmonary nodules with SUVs less than 1 or >4, 25 showed only a minor change between the 2 CAD schemes, indicating that the PET image characteristics played an essential role and that CT contributed relatively little information to the CAD scheme. However, of the 45 nodules with an SUV between 1 and 4, 27 showed a better performance for the CAD scheme that used PET/CT than for the CAD scheme that used PET alone, whereas only 6 demonstrated a decrease in performance with inclusion of the CT information. These facts indicate that CT features contributed significantly to distinguishing between benign and malignant nodules when SUV alone was not effective (between 1 and 4).

Figure 12 shows CT (Fig. 12A) and FDG-PET (Fig. 12B) images of a malignant nodule. Although PET in Figure 12B shows minimal FDG uptake by the nodule, CT in Figure 12A shows typical malignant patterns and was thus used to correct the negative finding in PET. The computer output based on FDG-PET alone indicated a negative finding with a low likelihood of malignancy of 0.27. By integrating PET with CT, the computed likelihood of malignancy was increased to 0.84.

CT can also be used to correct false-positive findings of FDG-PET. PET in Figure 13B shows high FDG uptake (false positive) for a benign nodule. However, CT in Figure 13A shows a characteristic benign pattern and was thus used to correct the false-positive finding in PET. The computed likelihood of malignancy for PET alone was high (0.78) and indicated a false-positive finding. When additional CT features were used, the likelihood of malignancy decreased to 0.29 and indicated a correct negative finding for the benign nodule. Therefore, radiologists could benefit from the CAD scheme for some lung nodules that are difficult to diagnose.

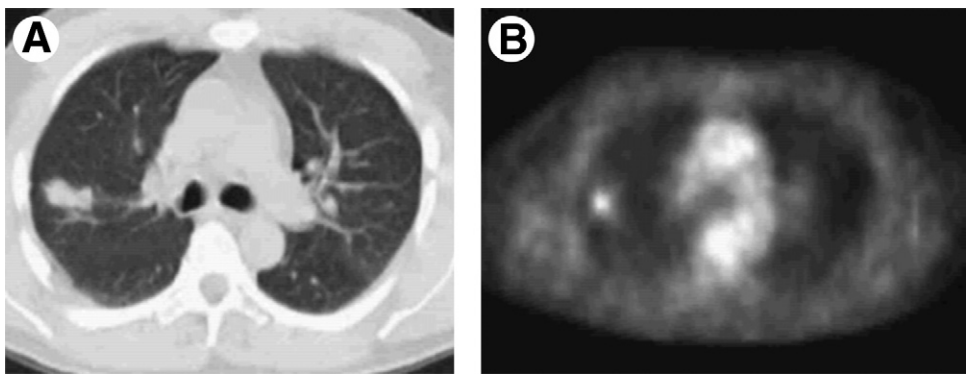

Figure 13 (A) CT and (B) FDG-PET scan of a 51-year-old man with a benign nodule that resolved after antibiotic therapy. By use of CT features, the computed likelihood of malignancy was improved (decreased) from 0.78 (an indication of cancer, PET alone) to 0.29 (an indication of a benign nodule, PET + CT).

Conclusions

A number of CAD techniques, such as temporal subtraction augmented by "artificial intelligence" algorithms, such as ANNs, have been developed and successfully applied to most radiologic modalities, including plain radiography, conventional scintigraphy, ultrasound, PET, CT, and magnetic resonance image and have demonstrated their utility in the detection of lesions and also the diagnosis of several benign and malignant pathologies. Some of these techniques are now in routine clinical use, most notably in mammography and to a lesser extent thoracic radiology, with ongoing efforts to translate CAD research to the routine clinical realm in virtually every radiologic subspecialty. It is likely that soon, CAD will be integrated into PACS and will become a standard of care for diagnostic examinations in daily clinical work.

References

1. Freer TW, Ulissey MJ: Screening mammography with computer-aided detection: Prospective study of 12,860 patients in a community breast center. Radiology 220:781-786, 2001
2. Gur D, Sumkin JH, Rockette HE, et al: Changes in breast cancer detection and mammography recall rates after the introduction of a computer-aided detection system. J Natl Cancer Inst 96:185-190, 2004
3. Birdwell RL, Bandodkar P, Ikeda DM: Computer-aided detection with screening mammography in a university hospital setting. Radiology 236:451-457, 2005
4. Cupples TE, Cunningham JE, Reynolds JC: Impact of computer-aided detection in a regional screening mammography program. AJR Am J Roentgenol 185:944-950, 2005
5. Morton MJ, Whaley DH, Brandt KR, et al: Screening mammograms: Interpretation with computer-aided detection—prospective evaluation. Radiology 239:375-383, 2006
6. Dean JC, Ilvento CC: Improved cancer detection using computer-aided detection with diagnostic and screening mammography: Prospective study of 104 cancers. AJR Am J Roentgenol 187:20-28, 2006
7. Destounis SV, DiNitto P, Logan-Young W, et al: Can computer-aided detection with double reading of screening mammograms help decrease the false-negative rate? Initial experience. Radiology 232:578-584, 2004
8. Gilbert FJ, Astley SM, Gillan MG, et al: Single reading with computer-aided detection for screening mammography. N Engl J Med 359:1675-1684, 2008
9. Nishikawa RM, Haldemann RC, Papaioannou J, et al: Initial experience with a prototype clinical "intelligent" mammography workstation for computer-aided diagnosis. Proc SPIE 2434:65-71, 1995
10. Schmidt RA, Nishikawa RM, Osnis RB, et al: Computerized detection of lesions missed by mammography, in Doi K, et al (eds): Digital Mammography. Amsterdam, Elsevier Science, 1996, pp 105-110
11. Warren Burhenne LJ, Wood SA, D'Orsi CJ, et al: Potential contribution of computer-aided detection to the sensitivity of screening mammography. Radiology 215:554-562, 2000
12. Giger ML, Huo Z, Kupinski MA, et al: Computer-aided diagnosis in mammography, in Fitzpatrick JM, Sonka M (eds): The Handbook of Medical Imaging, Vol 2, Medical Imaging Processing and Analysis. Bellingham, WA, SPIE Press, 2000, pp 915-1004
13. Giger ML: Computerized analysis of images in the detection and diagnosis of breast cancer. Semin Ultrasound CT MRI 25:411-418, 2004
14. Erickson BJ, Bartholmai B: Computer-aided detection and diagnosis at the start of the third millennium. J Digit Imaging 15:59-68, 2002
15. Summers RM: Road maps for advancement of radiologic computer-aided detection in the 21st century. Radiology 229:11-13, 2003
16. Abe H, MacMahon H, Shiraishi J, et al: Computer-aided diagnosis in chest radiography. Semin Ultrasound CT MRI 25:432-437, 2004
17. Li Q, Li F, Armato SG III, et al: Computer-aided diagnosis in thoracic CT. Semin Ultrasound CT MRI 26:357-363, 2005
18. Yoshida H, Dachman AH: Computer-aided diagnosis for CT colonography. Semin Ultrasound CT MRI 25:404-410, 2004
19. Doi K, Giger ML, MacMahon H, et al: Computer-aided diagnosis: Development of automated schemes for quantitative analysis of radiographic images. Semin Ultrasound CT MRI 13:140-152, 1992
20. Doi K, MacMahon H, Giger ML, et al (eds): Computer Aided Diagnosis in Medical Imaging. Amsterdam, Elsevier, 1999, pp 3-560
21. Doi K, MacMahon H, Katsuragawa S, et al: Computer-aided diagnosis in radiology: Potential and pitfalls. Eur J Radiol 31:97-109, 1999
22. Doi K: Computer-aided diagnosis in digital chest radiography. Advances in Digital Radiography: RSNA Categorical Course in Diagnostic Radiology Physics Syllabus, Oak Brooks, RSNA, 2003, pp 227-236
23. Doi K: Overview on research and development of computer-aided diagnostic schemes. Semin Ultrasound CT MRI 25:404-410, 2004
24. Doi K: Current status and future potential of computer-aided diagnosis in medical imaging. Br J Radiol Spec Issue 78:S3-S19, 2005
25. Doi K: Diagnostic imaging over the last 50 years: Research and development in medical imaging science and technology. Phys Med Biol 51:R5-R27, 2006
26. Doi K: Computer-aided diagnosis in medical imaging: Historical review, current status and future potential. Comput Med Imaging Graph 31:198-211, 2007
27. Lodwick GS, Haun CL, Smith WE, et al: Computer diagnosis of primary bone tumor. Radiology 80:273-275, 1963
28. Meyers PH, Nice CM, Becker HC, et al: Automated computer analysis of radiographic images. Radiology 83:1029-1033, 1964
29. Winsbarg F, Elkin M, May J, et al: Detection of radiographic abnormalities in mammograms by means of optical scanning and computer analysis. Radiology 89:211-215, 1967
30. Kruger RP, Towns JR, Hall DL, et al: Automated radiographic diagnosis via feature extraction and classification of cardiac size and shape descriptors. IEEE Trans Biomed Eng 19:175-186, 1972
31. Kruger RP, Thompson WB, Turner AF: Computer diagnosis of pneumoconiosis. IEEE Tran Systems, Man, and Cybernetics 4:44-47, 1974
32. Toriwaki J, Suenaga Y, Negoro T, et al: Pattern recognition of chest x-ray images. Comp Graph Imaging Process 2:252-271, 1973
33. Engle RL: Attempt to use computers as diagnostic aids in medical decision making: A thirty-year experience. Perspect Biol Med 35:207-218, 1992
34. Warner EE, Mulshine JL: Lung cancer screening with spiral CT: Ttoward a working strategy. Oncol Williston Park 18:564-575, discussion: 578, 583-584, 587, 2004
35. Kaneko M, Eguchi K, Ohmatsu H, et al: Peripheral lung cancer: Screening and detection with low-dose spiral CT versus radiography. Radiology 201:798-802, 1996
36. Sone S, Takashima S, Li F, et al: Mass screening for lung cancer with mobile spiral computed tomography scanner. Lancet 351:1242-1245, 1998
37. Henschke CI, McCauley DI, Yankelevitz DF, et al: Early lung cancer action project: Overall design and findings from baseline screening. Lancet 354:99-105, 1999
38. Henschke CI, Yankelevitz DF, Mirtcheva R, et al: CT screening for lung cancer: Frequency and significance of part-solid and nonsolid nodules. AJR Am J Roentgenol 178:1053-1057, 2002
39. Li F, Sone S, Abe H, et al: Lung cancers missed at low-dose helical CT screening in a general population: Comparison of clinical, histopathologic, and imaging findings. Radiology 225:673-683, 2002
40. Armato SG III, Li F, Giger ML, et al: Lung cancer: Performance of automated lung nodule detection applied to cancers missed in a CT screening program. Radiology 225:685-692, 2002
41. Yoshida H, Masutani Y, MacEneaney P, et al: Computerized detection of colonic polyps at CT colonography on the basis of volumetric features: Pilot study. Radiology 222:327-336, 2002
42. Yoshida H, Näppi J, MacEneaney P, et al: Computer-aided diagnosis scheme for detection of polyps at CT colonography. Radiographics 22:963-979, 2002
43. Oken MM, Marcus PM, Hu P, et al: Baseline chest radiograph for lung cancer detection in the randomized Prostate, Lung, Colorectal and

Ovarian Cancer Screening Trial. J Natl Cancer Inst 97:1832-1839, 2005
44. Shiraishi J, Li Q, Appelbaum D, et al: Development of a computer-aided diagnostic scheme for detection of interval changes in successive whole-body bone scans. Med Phys 34:25-36, 2007
45. Shiraishi J, Appelbaum D, Pu Y, et al: Usefulness of temporal subtraction images for identification of interval changes in successive whole-body bone scans: JAFROC analysis of radiologists' performance. Acad Radiol 14:959-966, 2007
46. Shiraishi J, Appelbaum D, Pu Y, et al: Clinical utility of temporal subtraction images in successive whole-body bone scans: Evaluation in a prospective clinical study. J Digit Imaging 24:680-687, 2011
47. Nie Y, Li Q, Li F, et al: Integrating PET and CT information to improve diagnostic accuracy for lung nodules: A semiautomatic computer-aided method. J Nucl Med 47:1075-1080, 2006
48. Kano A, Doi K, MacMahon H, et al: Digital image subtraction of temporally sequential chest images for detection of interval change. Med Phys 21:453-461, 1994
49. Difazio MC, MacMahon H, Xu XW, et al: Digital chest radiography: Effect of temporal subtraction images on detection accuracy. Radiology 202:447-452, 1997
50. Kakeda S, Nakamura K, Kamada K, et al: Improved detection of lung nodules by using a temporal subtraction technique. Radiology 224: 145-151, 2002
51. Kakeda S, Kamada K, Hatakeyama Y, et al: Effect of temporal subtraction technique on interpretation time and diagnostic accuracy of chest radiography. AJR Am J Roentgenol 187:1253-1259, 2006
52. Ishida T, Katsuragawa S, Nakamura K, et al: Iterative image warping technique for temporal subtraction of sequential chest radiographs to detect interval change. Med Phys 26:1320-1329, 1999
53. Li Q, Katsuragawa S, Doi K: Improved contralateral subtraction images by use of elastic matching technique. Med Phys 27:1934-1942, 2000
54. Abe H, Ishida T, Shiraishi J, et al: Effect of temporal subtraction images on radiologists' detection of lung cancer on CT: Results of the observer performance study with use of film computed tomography images. Acad Radiol 11:1337-1343, 2004
55. Itai Y, Kim H, Ishikawa S, et al: Development of a voxel-matching technique for substantial reduction of subtraction artifacts in temporal subtraction images obtained from thoracic MDCT. J Digit Imaging 23: 31-38, 2010
56. National Lung Screening Trial Research Team, Aberle DR, Berg CD, et al: The National Lung Screening Trial: Overview and study design. Radiology 258:243-253, 2011
57. Chakraborty DP, Berbaum KS: Observer studies involving detection and localization: Modeling, analysis, and validation. Med Phys 31: 2313-2330, 2004
58. Zheng B, Chakraborty DP, Rockette HE, et al: A comparison of two data analyses from two observer performance studies using Jackknife ROC and JAFROC. Med Phys 32:1031-1034
59. Chakraborty DP, Winter LH: Free-response methodology: Alternate analysis and a new observer-performance experiment. Radiology 174: 873-881, 1990
60. Dorfman DD, Berbaum KS, Metz CE: Receiver operating characteristic rating analysis. Generalization to the population of readers and patients with the jackknife method. Invest Radiol 27:723-731, 1992
61. Giger ML, Doi K, MacMahon H: Image feature analysis and computer-aided diagnosis in digital radiography. 3. Automated detection of nodules in peripheral lung fields. Med Phys 15:158-166, 1988
62. Wu YC, Doi K, Giger ML, et al: Reduction of false positives in computerized detection of lung nodules in chest radiographs using artificial neural networks, discriminant analysis, and a rule-based scheme. J Digit Imaging 7:196-207, 1994
63. Asada N, Doi K, MacMahon H, et al: Potential usefulness of an artificial neural network for differential diagnosis of interstitial lung diseases: Pilot study. Radiology 177:857-860, 1990
64. Ashizawa K, Ishida T, MacMahon H, et al: Artificial neural networks in chest radiography: Application to the differential diagnosis of interstitial lung disease. Acad Radiol 6:2-9, 1999
65. Ashizawa K, MacMahon H, Ishida T, et al: Effect of an artificial neural network on radiologists' performance in the differential diagnosis of interstitial lung disease using chest radiographs. AJR Am J Roentgenol 172:1311-1315, 1999
66. Abe H, Ashizawa K, Li F, et al: Artificial neural networks (ANNs) for differential diagnosis of interstitial lung disease: Results of a simulation test with actual clinical cases. Acad Radiol 11:29-37, 2004
67. Fukushima A, Ashizawa K, Yamaguchi T, et al: Application of an artificial neural network to high-resolution CT: Usefulness in differential diagnosis of diffuse lung disease. AJR Am J Roentgenol 183:297-305, 2004
68. Nakamura K, Yoshida H, Engelmann R, et al: Computerized analysis of the likelihood of malignancy in solitary pulmonary nodules with use of artificial neural networks. Radiology 214:823-830, 2000
69. Matsuki Y, Nakamura K, Watanabe H, et al: Usefulness of an artificial neural network for differentiating benign from malignant pulmonary nodules on high-resolution CT: Evaluation with receiver operating characteristic analysis. AJR Am J Roentgenol 178:657-663, 2002
70. Aoyama M, Li Q, Katsuragawa S, et al: Automated computerized scheme for distinction between benign and malignant solitary pulmonary nodules on chest images. Med Phys 29:701-708, 2002
71. Lo SC, Freedman MT, Lin JS, et al: Automatic lung nodule detection using profile matching and back-propagation neural network techniques. J Digit Imaging 6:48-54, 1993
72. Zhang W, Doi K, Giger ML, et al: Computerized detection of clustered microcalcifications in digital mammograms using a shift-invariant artificial neural network. Med Phys 21:517-524, 1994
73. Wu Y, Giger ML, Doi K, et al: Artificial neural networks in mammography: Application to decision making in the diagnosis of breast cancer. Radiology 187:81-87, 1993
74. Baker JA, Kornguth PJ, Lo JY, et al: Breast cancer: Prediction with artificial neural network based on BI-RADS standardized lexicon. Radiology 196:817-822, 1995
75. Lo JY, Baker JA, Kornguth PJ, et al: Predicting breast cancer invasion with artificial neural networks on the basis of mammographic features. Radiology 203:159-163, 1997
76. Sahiner B, Chan HP, Petrick N, et al: Classification of mass and normal breast tissue: A convolution neural network classifier with spatial domain and texture images. IEEE Trans Med Imaging 15:598-610, 1996
77. Errejon A, Crawford ED, Dayhoff J, et al: Use of artificial neural networks in prostate cancer. Mol Urol 5:153-158, 2001
78. Tourassi GD, Floyd CE, Sostman HD, et al: Acute pulmonary embolism: Artificial neural network approach for diagnosis. Radiology 189: 555-558, 1993
79. Tourassi GD, Floyd CE, Sostman HD, et al: Artificial neural network for diagnosis of acute pulmonary embolism: Effect of case and observer selection. Radiology 194:889-893, 1995
80. Jain AK, Mao J, Mohiuddin KM: Artificial neural networks: A tutorial. Computer 29:31-44, 1996
81. Bishop CM: Neural networks and their applications. Rev Sci Instrum 65:1803-1832, 1994
82. Dayhoff JE, DeLeo JM: Artificial neural networks: Opening the black box. Cancer 91:1615-1635, 2001
83. Basheer IA, Hajmeer M: Artificial neural networks: Fundamentals, computing, design, and Application. J Microbiol Methods 43:3-31, 2000